Philosophical Magazine
Vol. 91, No. 11, 11 April 2011, 1557–1567

Taylor & Francis
Taylor & Francis Group

The effect of a transverse electric field on the electronic properties of an armchair carbon nanoscroll

T.S. Li[a]*, M.F. Lin[b] and J.Y. Wu[b]

[a]*Department of Electrical Engineering, Kun Shan University, Tainan, Taiwan, Republic of China;* [b]*Department of Physics, National Cheng Kung University, Tainan, Taiwan, Republic of China*

(*Received 20 April 2010; final version received 11 November 2010*)

In this work, we use the tight-binding model to study the low-energy electronic properties of carbon nanoscrolls subject to the influences of a transverse electric field. A carbon nanoscroll can be considered as an open-ended spirally wrapped graphene nanoribbon. The inter-wall interactions will alter the subband curvature, create additional band-edge states, modify the subband spacing or energy gap, and separate the partial flat bands. Furthermore, the energy band symmetry about the Fermi level is lifted by such interactions. The truncated Archimedean spiral $\rho = r_a\theta + r$ is used to describe the spiral structures of carbon nanoscrolls. The energy gap is found to oscillate significantly with r, and exhibits complete energy gap modulations. With the inclusion of a transverse electric field, the band structures are further altered. Inter-wall hoppings will cause electron transfers between different atoms leading to distortions of the electron wavefunctions. The main features of the energy dispersions are directly reflected in the density of states. The numbers, heights, and energies of the density of states peaks are dependent on the electric field strength.

Keywords: electronic properties; carbon nanostructures; carbon nanoscrolls

1. Introduction

Carbon is a very versatile element. In nature, carbon-based materials can be formed in different dimensionalities, such as diamond (three dimensional, 3D), graphene (2D), carbon nanotubes (1D) [1,2], and fullerenes (0D). For graphene, carbon nanotubes, and fullerenes, the sp^2 hybridization of hexagonal or pentagonal carbon networks is essential to model their electronic structures. Graphene is a flat monolayer honeycomb lattice. Rolling a graphene sheet into a seamless cylinder, a single-walled carbon nanotube (SWCNT) is formed. The geometric structure of a SWCNT is uniquely determined by the chiral vector $\vec{C}_h = m\vec{a}_1 + n\vec{a}_2$, or simply (m, n), where $\vec{a}_1$ and $\vec{a}_2$ are the primitive lattice vectors of the graphite sheet; m and n are integers. Its peculiar electronic properties have stimulated extensive research activities since it was discovered by Iijima in 1991 [1]; whether a SWCNT is metallic

*Corresponding author. Email: tsli@mail.ksu.edu.tw

ISSN 1478–6435 print/ISSN 1478–6443 online

DOI: 10.1080/14786435.2010.543091
http://www.informaworld.com

or semiconducting depends critically on how the graphene sheet is rolled up. A (m, n) SWCNT can be classified into three categories according to its energy gap [3–5]: (I) a gapless metal for $m = n$; (II) a narrow-gap semiconductor with $E_g \propto R^{-2}$ for $2m + n = 3I$ and $m \neq n$ (I is an integer); and (III) a moderate-gap semiconductor with $E_g \propto R^{-1}$ for $2m + n \neq 3I$, where R is the tube radius. The main difference between type-I and type-II SWCNTs stems from the curvature effects (the misorientation of the $2p_z$ orbitals and the hybridization of π and σ electrons). This predicted energy-gap behavior has been verified by measurements of scanning tunneling spectroscopy (STS) [6–9] and optical absorptions [10,11].

When flat graphene is patterned into a narrow ribbon, a graphene nanoribbon (GNR) will then be obtained. Graphene nanoribbons can be realized either by cutting mechanically exfoliated graphenes [12], or by patterning graphenes with lithographic techniques [13,14]. In zigzag nanoribbons, there are strongly localized states at the zigzag edges, called "edge states" which give rise to the partial flat bands in the range $2/3 \leq k \leq 1$ [15], where k is the wavevector in units of π/a. $a = \sqrt{3}b$, and $b = 1.42$ Å is the C–C bond length. At $k = 1$, the electron wavefunction is perfectly localized at the zigzag edge. When k deviates from 1, the wavefunction gradually penetrates and decays exponentially towards the inner sites.

A carbon nanoscroll (CNS) can be considered as an open-ended spirally wrapped GNR (Figure 1). Unlike SWCNT, a CNS cannot be uniquely determined by the chiral vector. It previously carried the name of a Swiss-roll multi-walled carbon nanotube [16]. CNSs were first reported by Bacon in 1960 [17]. Due to the advance of synthesis techniques, CNSs can now be produced in large quantities [18,19]. Theoretical calculations on CNSs were first performed by employing continuum elasticity theory to analyze the structure and stability of CNSs [20–22]. However, this approach cannot describe atomic-level structural features. Recently, Braga and

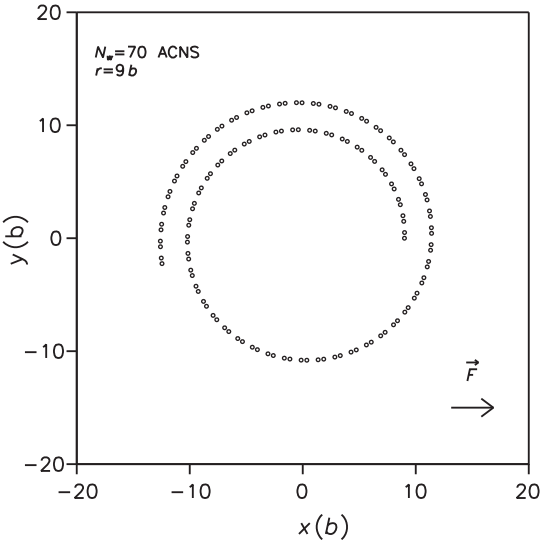

Figure 1. Cross-sectional view of a $N_w = 70$ armchair carbon nanoscroll.

coworkers used molecular dynamics simulations to investigate the formation and stability of nanoscrolls [23].

2. The tight-binding method

Graphene nanoribbons are finite-width carbon stripes cut out from graphene. There are two basic types of graphene nanoribbons, namely, armchair ribbons and zigzag ribbons. The former and latter are confined by a pair of parallel armchair and zigzag edges on both sides, respectively. The ribbon width N_w denotes the number of dimer lines for armchair ribbons and the number of zigzag lines for zigzag ribbons. There are $2N_w$ carbon atoms ($2N_w$ $2p_z$ orbitals) in a primitive unit cell. We use the single-orbital nearest-neighbor tight-binding Hamiltonian to calculate the band structure formed by the π orbitals. The wavefunction is the linear superposition of the $2N_w$ tight-binding functions. The Hamiltonian, which is built from the subspace spanned by these tight-binding functions, is a $2N_w \times 2N_w$ Hermitian matrix. For a zigzag GNR, it is given by

$$H_{ij} = \begin{cases} 2\gamma_0 \cos(k\pi/2) & \text{if } j = i+1;\ j \text{ is even,} \\ \gamma_0 & \text{if } j = i+1; j \text{ is odd,} \\ 0 & \text{otherwise.} \end{cases} \quad (1)$$

In this paper, the dangling bonds on the edge sites are assumed to be terminated by hydrogen atoms, and the dangling bonds do not contribute to the low-energy electronic states [14]. Zigzag GNRs are gapless. Armchair GNRs with $N_w = 3I+2$ are also gapless, and those with $N_w \neq 3I+2$ are semiconductors. Details of the geometric and electronic structures of graphene nanoribbons are given in [15,24,25].

When a flat GNR is spirally wrapped into a CNS, the $2p_z$ orbitals are no longer parallel to each other, and curvature effects need to be taken into account. In this calculation, the π bonding $V_{pp\pi}$ ($=-2.66$ eV $=-\gamma_0$) and σ bonding $V_{pp\sigma}$ ($=6.38$ eV) are considered in the nearest neighbor hoppings. The Hamiltonian is

$$\mathcal{H} = -\sum_{i,j} t_{i,j} c_i^+ c_j - W \sum_{i,j} t_{i,j} e^{(d_{opt}-d_{ij})/\delta} c_i^+ c_j, \quad (2)$$

where $t_{i,j}$ is the transfer integral. Only hoppings between the nearest neighbors are considered. The inter-wall hoppings are handled in the second term. Such hoppings are assumed to decay exponentially with inter-atom distance d_{ij}, according to Ahn's model originally proposed for "Russian-doll" type multi-walled carbon nanotubes [26]. $\delta = 0.45$ Å and the parameter W is chosen to be 1/8. c_i^+ and c_j are the creation and annihilation operators at sites i and j, respectively. In our previous work, we have used this model in nanotube–ribbon hybrid systems [27,28]. In the presence of a transverse electric field, the on-site energy of the ith carbon atom in a CNS will be perturbed by the amount $\delta E = -eFx_i$, where x_i is the coordinate of the ith carbon atom along the field direction. After diagonalizing the Hamiltonian, the state energy $E^{c,v}(F)$ can be obtained. The superscripts, c and v, represent the conduction band and the valence band, respectively.

Following the nomenclature given in Braga's paper [23], the CNS obtained by rolling a zigzag GNR is an armchair carbon nanoscroll (ACNS), while that formed by wrapping an armchair GNR is a zigzag carbon nanoscroll (ZCNS). For GNRs, the names of zigzag GNR and armchair GNR arise from the shape of the confining edges. On the other hand, for CNSs, the classification of zigzag CNS and armchair CNS are the shape of the cross-sectional spiral. In this study, we use the truncated Archimedean spiral $\rho = r_a\theta + r$ to describe the spiral structures of CNSs, where ρ and θ are the usual polar coordinates. r_a and r are non-zero constants. r_a determines the inter-wall spacing d_{inter} as $d_{\text{inter}} = 2\pi r_a$. d_{inter} is chosen to be 3.4 Å, which is similar to the inter-layer distance of the Russian doll or graphite. The cross-sectional view of a $N_w = 70$ ACNS is shown in Figure 1.

3. Electronic properties

The $N_w = 70$ ACNS is chosen to be a model study. The energy dispersion relationships of its zigzag GNR counterpart are also shown for comparison (Figures 2a and b). Zigzag GNR is gapless, and has partial flat bands at the Fermi level. The energy bands are symmetric about the Fermi level $E_F = 0$. After rolling into an ACNS, the band structures are only slightly modified if inter-wall interactions are neglected (Figure 2a), and the subbands are still symmetric about the Fermi level. This indicates that the curvature effect has little influence on the energy bands of nanoscrolls, and will not alter the subband symmetry about E_F. After switching on the inter-wall hoppings, the partial flat bands are separated, and the energy band symmetry about $E_F = 0$ is lifted. Such hoppings will also change the subband curvature. Furthermore, the band-gap may be opened or closed as r varies. At $r = 9\ b$, the subband curvatures are different from those of the GNR. The partial flat bands become detached and deformed, and an energy gap of $\approx 0.008\ \gamma_0$ is opened (Figure 2b). At $r = 13\ b$, the separated partial flat bands are a little wavy. New band-edge states are developed around $k = 2/3$. The band-gap is approximately $0.005\ \gamma_0$ (Figure 2c). At $r = 14.9\ b$, the partial flat bands oscillate impressively, and produce several additional band-edge states (Figure 2d). The conduction and valence bands nearest to E_F change into almost linear bands in the vicinity of $k = 2/3$ and touch one another, resulting in a zero energy gap.

With the inclusion of a transverse electric field, the band structures are further altered. By comparing the dispersion relationships at zero F (Figure 2b) and non-zero F (Figure 3), one can see that the electric field will modify the subband curvature, create new band-edge states, and change the subband spacing. The partial flat bands are pushed away from E_F and transform into distorted parabolic bands. In particular, the lower partial flat band is farther away from E_F than the upper one. Furthermore, the band-gap switches from direct (the k-vectors of the minimal-energy state in the conduction band, and the maximal-energy state in the valence band are the same) to indirect as F grows. At $F = 0.006\ \gamma_0/e$ Å, the lower partial flat band is pushed away from E_F and starts to mix with an originally parabolic band (Figure 3a). The band-gap is direct. As F increases to $0.009\ \gamma_0/e$ Å, the highest valence band changes from a single-peak to a double-peak structure because of band-mixing (Figure 3b). Additional band-edge states are created and the band-gap

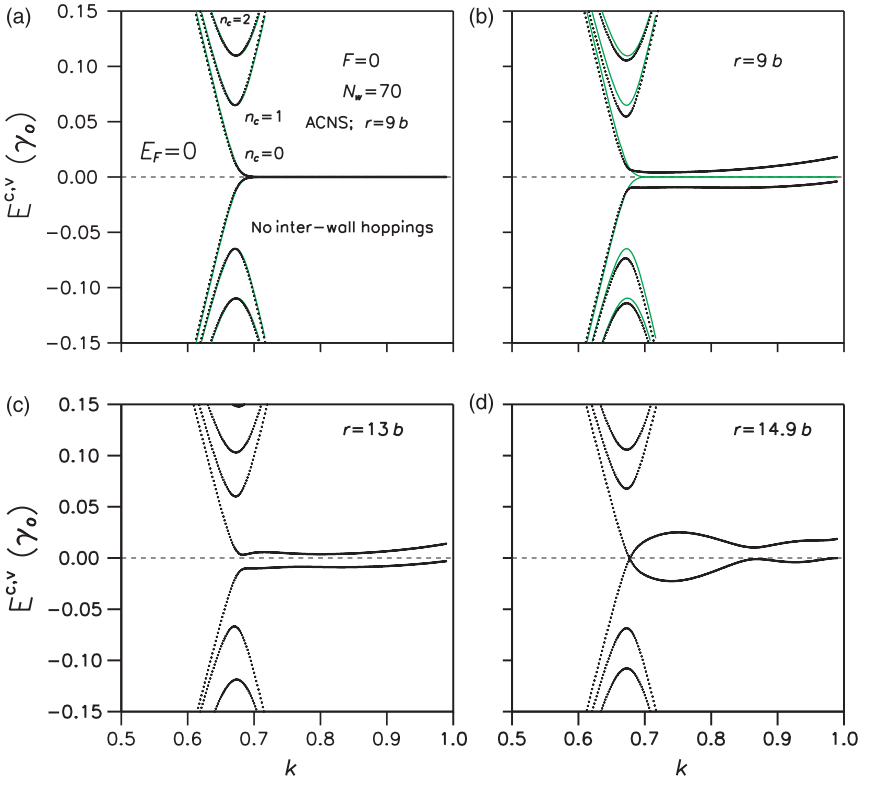

Figure 2. The low-energy subbands of the $N_w = 70$ ACNS, at (a) $r = 9\ b$, without inter-wall hoppings, (b) $r = 9\ b$, with inter-wall hoppings, (c) $r = 13\ b$, and (d) $r = 14.9\ b$. The electric field strength F is zero. In (a) and (b), the subbands of the $N_w = 70$ zigzag graphene nanoribbon are shown as solid lines (green online) for comparison.

is indirect. Band-mixing in the upper partial flat band becomes obvious. At $F = 0.012\ \gamma_0/e$ Å, the lowest conduction band begins to alter from a single-dip to a double-dip structure (Figure 3c). The double-peak structure of the highest valence band is getting more obvious. In addition, the band-gap is indirect. At $F = 0.015\ \gamma_0/e$ Å, the band-mixing is strong, and many new band-edge states are created (Figure 3d). The lowest conduction band and the highest valence band touch E_F at different k's, resulting in a zero and indirect band-gap.

The energy gap of an ACNS depends sensitively on r and is oscillatory (Figure 4a). It will exhibit complete energy gap modulations (E_g switches back and forth between non-zero and zero values) with varying r. When r exceeds 15.4 b, the ACNS is gapless for all r's. At large r, there are no inter-wall interactions, and the dispersion relationships of ACNSs are nearly the same as those of zero gap zigzag GNRs. At $r = 15.4\ b$, the inner and outer walls start to overlap. As r reduces, the overlapping region increases, and more atoms are involved in the inter-wall hoppings. In addition, the stacking on the overlapping region also changes with varying r. Consequently, E_g is oscillatory with r. The F-dependence of the energy gap is shown in Figure 4b. For $r = 9\ b$, E_g initially increases with F,

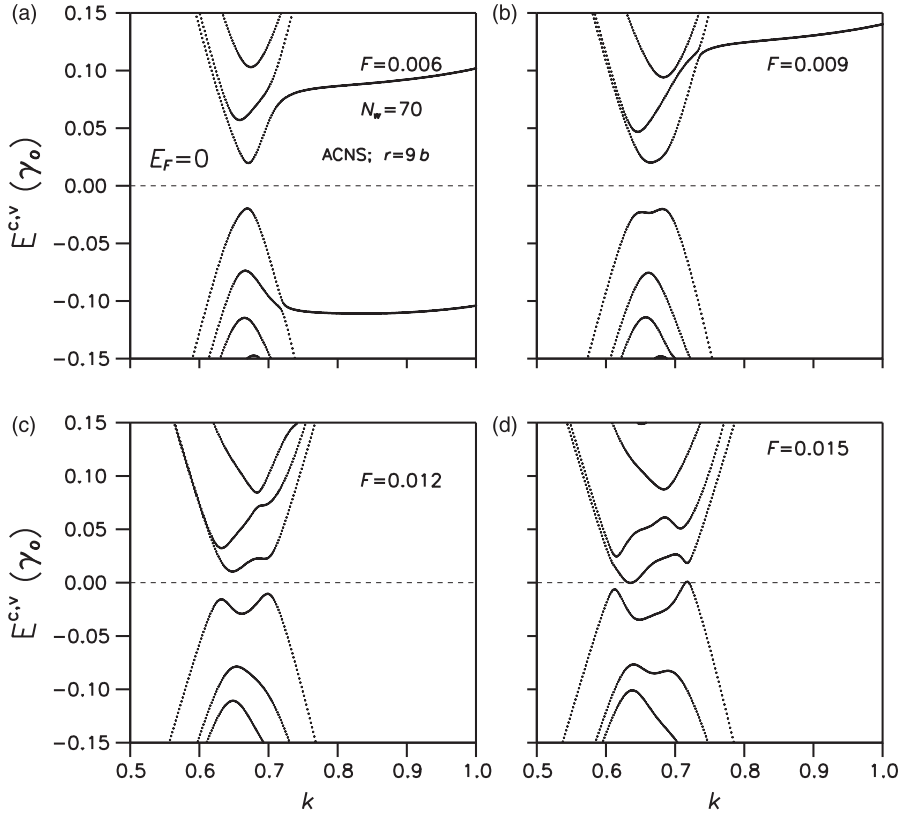

Figure 3. The low-energy subbands of the $N_w = 70$ ACNS, at $r = 9\ b$ and (a) $F = 0.006\ \gamma_0/e$ Å, (b) $F = 0.009\ \gamma_0/e$ Å, (c) $F = 0.012\ \gamma_0/e$ Å, and (d) $F = 0.015\ \gamma_0/e$ Å.

reaches a maximum value, and then decreases to zero. For $r = 11\ b$, the band-gap is zero when F is small, then grows with incrementing F. It arrives at a peak value, then drops and rises sequentially a few times. For $r = 13\ b$, the energy gap takes the maximum value at $F = 0$, then diminishes with rising F, and is zero at large F. For $r = 15\ b$, there is a small band-gap of $\approx 0.003\ \gamma_0$ at $F = 0$. The gap shrinks with growing F, and stays at zero for F greater than $0.0003\ \gamma_0/e$ Å.

The features of the ground-state wavefunctions are investigated. The envelope function Ψ_{n_c} of a zigzag GNR can be decomposed into four sub-envelope functions: $\Psi_{n_c} = \Psi_{n_c}(A^o) + \Psi_{n_c}(A^e) + \Psi_{n_c}(B^o) + \Psi_{n_c}(B^e)$ [29], where A^o, A^e, B^o, and B^e represent A or B atoms at the *odd* or *even* zigzag lines of the zigzag GNR. $\Psi_{n_c}(A^e) = -\Psi_{n_c}(A^o)$ and $\Psi_{n_c}(B^e) = -\Psi_{n_c}(B^o)$. The subband index n_c $(= 0, 1, 2, 3, \ldots)$ characterizes the conduction bands counting from E_F. At $F = 0$ and $k = 1$, $\Psi_{n_c=0}(A^o)$ and $\Psi_{n_c=0}(A^e)$ are the localized edge states which are perfectly localized at the zigzag edge (not shown). At $k = 11/12$, $\Psi_{n_c=0}(A^o)$ and $\Psi_{n_c=0}(A^e)$ are found to be still mostly confined at one of the zigzag edges (Figure 5a). When k departs further from 1, they gradually penetrate and decay exponentially towards the inner sites. At $k = 2/3$, $\Psi_{n_c=0}(A^o)$ and $\Psi_{n_c=0}(A^e)$ of the GNR are no longer exponentially decaying functions and spread more widely

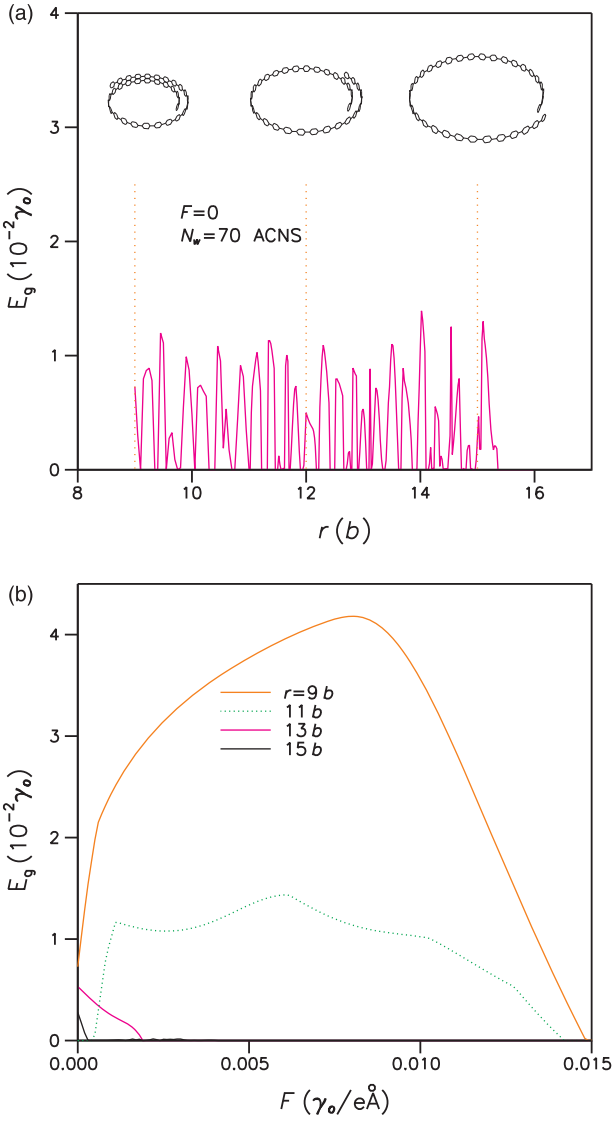

Figure 4. The energy gap of the $N_w = 70$ ACNS versus (a) r, and (b) F with $r = 9\ b$, 11 b, 13 b and 15 b. The insets in (a) show the geometries of the $N_w = 70$ ACNS with $r = 9\ b$, 12 b, and 15 b. In (a), the increment step of r is 0.05 b.

in space than the wavefunctions at $k = 3/4$, 5/6, or 11/12. At $k = 5/6$ or 11/12, $\Psi_{n_c=0}(B^o)$ is zero, signifying that the electrons only reside on A atoms. At $k = 3/4$, $\Psi_{n_c=0}(B^o)$ is non-zero and settles mainly at another edge. Finally, $\Psi_{n_c=0}(B^o)$ stretches out at $k = 2/3$. After rolling up into a scroll, the CNS electron wavefunctions almost coincide with the GNR wavefunctions if inter-wall interactions are turned off (Figures 5a and b). It demonstrates that the curvature effect hardly alters the electron distribution. After turning on the inter-wall interactions, the electron wavefunctions

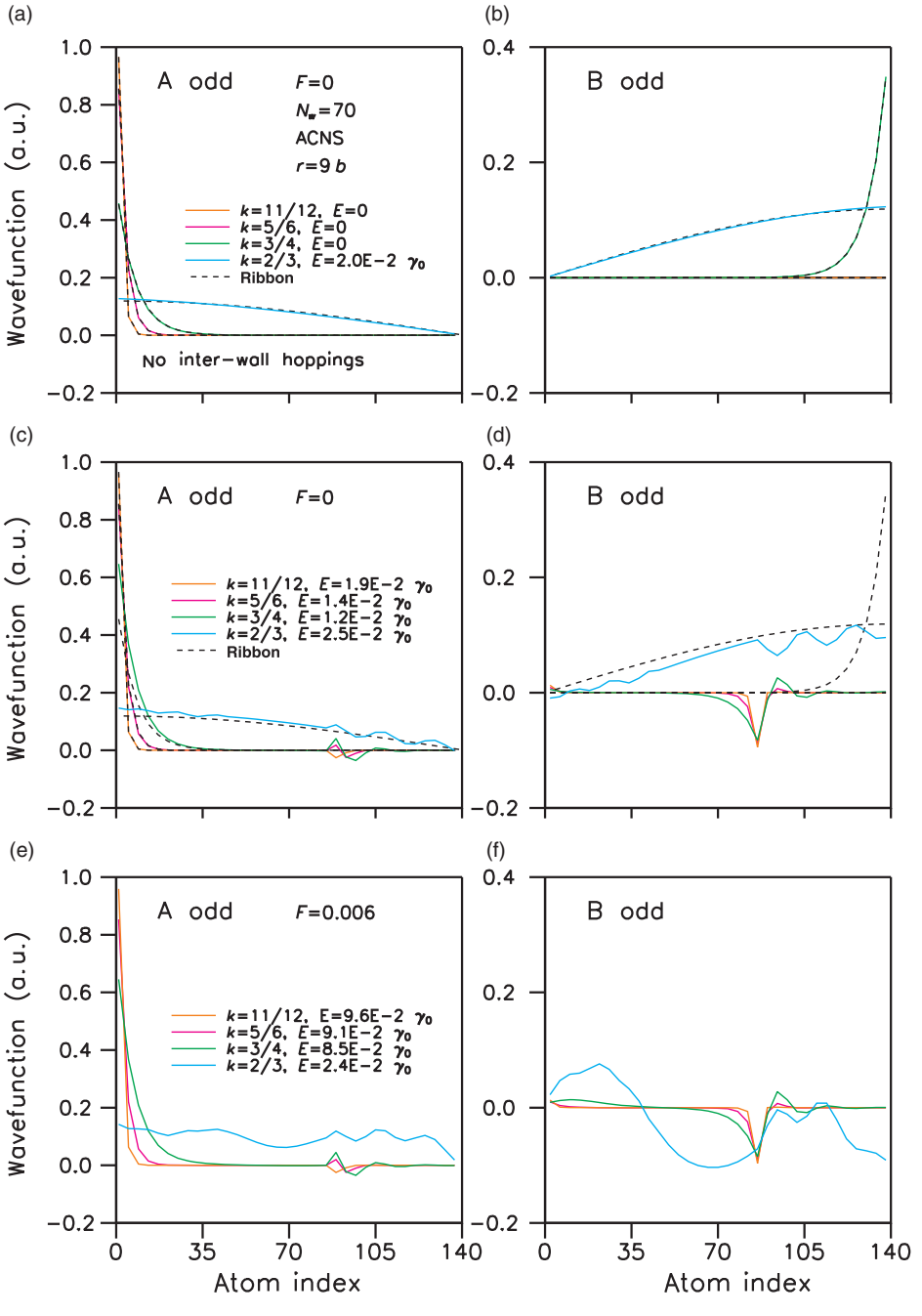

Figure 5. The $n_c = 0$ envelope functions of the $N_w = 70$ ACNS at $k = 11/12$, 5/6, 3/4, and 2/3 on (a) A odd sites with $F = 0$, and no inter-wall hoppings, (b) B odd sites with $F = 0$, and no inter-wall hoppings, (c) A odd sites with $F = 0$, and inter-wall hoppings, (d) B odd sites with $F = 0$, and inter-wall hoppings, (e) A odd sites with $F = 0.006\ \gamma_0/e$ Å, and (f) B odd sites with $F = 0.006\ \gamma_0/e$ Å. In (a), (b), (c), and (d), the envelope functions of the $N_w = 70$ zigzag graphene nanoribbon are shown as dashed lines for comparison.

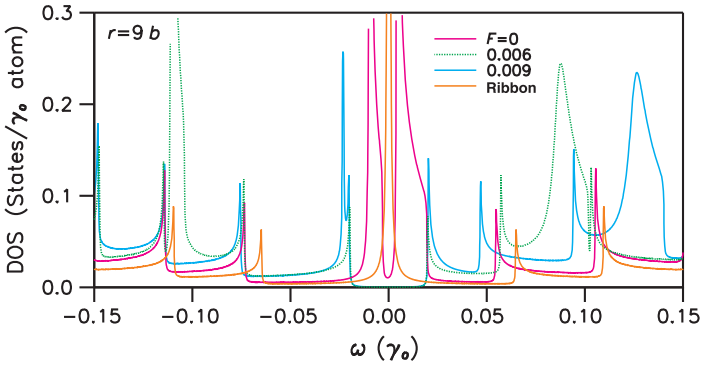

Figure 6. Density of states per atom of the $N_w = 70$ ACNS at different F. The DOS of the $N_w = 70$ zigzag graphene nanoribbon is also shown for comparison.

change and deviate significantly from the GNR wavefunctions (Figures 5c and d). With inter-wall hoppings, there are electron transfers between A and B atoms, also between the inner-wall and the outer-wall atoms. At $k = 2/3$, the ACNS wavefunction on A sites is larger than that of the GNR sites, whereas it is smaller on B sites, indicating that there are electron transfers from B to A atoms. At $k = 3/4$, $\Psi_{n_c=0}(A^o)$ of the GNR is mostly located at one of the edges, while $\Psi_{n_c=0}(B^o)$ is located at another one. After rolling up into a scroll, the electrons on B sites migrate from the edge to other A and B atoms, elevating $\Psi_{n_c=0}(A^o)$ and causing kink structures in the wavefunctions. At $k = 5/6$ or $11/12$, $\Psi_{n_c=0}(B^o)$ of the GNR is zero. Inter-wall hoppings will induce the electrons on A sites to move from the edge to other A and B atoms. The $\Psi_{n_c=0}(B^o)$ of ACNSs becomes non-zero. An electric field with $F = 0.006\ \gamma_0/e\,\text{Å}$ change the CNS electron wavefunctions considerably (Figures 5e and f). Finally, the electron transfers between different atoms are further enhanced by the electric field. The electron wavefunctions are related to other interesting problems such as the optical properties and Coulomb excitations in carbon nanoscrolls.

Many of these electronic properties will be reflected in the density of states (DOS) which is defined as

$$D(\omega) = \sum_{c,v} \int_{1\text{st BZ}} \frac{\mathrm{d}k}{(2\pi)^2} \frac{\Gamma}{(\omega - E^{c,v})^2 + \Gamma^2}, \tag{3}$$

where $\Gamma = 2 \times 10^{-4}\ \gamma_0$ is the broadening parameter. In CNSs, there are many 1D parabolic subbands. Consequently, the DOS will exhibit many divergent peaks in the asymmetric square-root form (the van Hove singularities) (Figure 6). The peak energies correspond to the band-edge state energies (E_{ed}'s). The height of the peak is proportional to the inverse square root of the subband curvature (or the square root of the electron effective mass). When the subbands are concave downward and upward, the associating DOS would exhibit a divergent peak in the $1/\sqrt{\omega - E_{\text{ed}}}$ and $1/\sqrt{E_{\text{ed}} - \omega}$ form, respectively. Apart from the asymmetric square-root form divergent peaks, there are also prominent divergent peaks near E_F, due to the partial

flat bands. The DOS of a $N_w = 70$ zigzag GNR is symmetric about E_F. After rolling up the GNR into a scroll, the DOS becomes asymmetric. This symmetry breaking is also caused by the inter-wall interactions just like that in energy bands mentioned previously. Moreover, such interactions separate the partial flat bands and change the single prominent divergent peak at E_F into double peaks. The addition of an electric field changes the energy dispersions considerably, and creates new band-edge states. Therefore, the main features of the DOS, such as the numbers, the heights, and the positions of the divergent peaks, are dependent on the electric field strength F. F will also modify the partial flat bands and consequently the locations and extent of the prominent divergent peaks. For example, an electric field with $F = 0.006\ \gamma_0/e\,\text{Å}$ shifts the upper prominent divergent peak to $0.09\ \gamma_0$, and the shape of the peak is also different from the one at $F = 0$. The peak is further elevated to $0.13\ \gamma_0$ at $F = 0.009\ \gamma_0/e\,\text{Å}$. The DOS peaks can be directly probed by STS conductance measurements [6–9], and they are also closely related to the absorption peaks in optical spectroscopy experiments [10,11]. Therefore, our calculated results can be validated experimentally. Finally, we wish to make a few comments about the geometry of the nanoscrolls. The $N_w = 70$ armchair nanoscroll is chosen as a model study. The electronic properties of armchair nanoscrolls with other N_w's are similar to those of $N_w = 70$. According to Braga's computation results [23], the Archimedean spiral scroll, which is adopted in this work, is a stable configuration.

4. Concluding remarks

In conclusion, the tight-binding model has been used to explore the low-energy electronic properties of carbon nanoscrolls subject to the influences of a transverse electric field. The energy dispersions, electron wavefunctions, and DOS depend sensitively on the inter-wall interactions and the electric field strength. The energy band symmetry about the Fermi level is lifted by such interactions, and the energy gap is found to oscillate significantly with r. In the presence of a transverse electric field, the partial flat bands are pushed away from the Fermi level and turn into distorted parabolic bands. In addition, the band-gap changes from direct to indirect as the field strength rises. With inter-wall hoppings, there are electron transfers between A and B atoms, also between the inner-wall and the outer-wall atoms. Consequently, the electron wavefunctions are modified. Such transfers also depend on F. The electron wavefunctions are related to other interesting problems such as the optical properties and Coulomb excitations in carbon nanoscrolls. The main features of the band structure are directly reflected in the DOS. The numbers, heights, and energies of the DOS peaks are found to be dependent on the electric field strength. These theoretical predictions can be validated by STS and optical absorption measurements.

Acknowledgements

This work was supported in part by the National Science Council of Taiwan, the Republic of China under Grant No. NSC 98-2112-M-168-001-MY2.

References

[1] S. Iijima, Nature 354 (1991) p.56.
[2] R. Saito, M. Fujita, G. Dresselhaus and M.S. Dresselhaus, Appl. Phys. Lett. 60 (1992) p.2204.
[3] N. Hamada, S.I. Sawada and A. Oshiyama, Phys. Rev. Lett. 68 (1992) p.1579.
[4] C.L. Kane and E.J. Mele, Phys. Rev. Lett. 78 (1997) p.1932.
[5] F.L. Shyu and M.F. Lin, J. Phys. Soc. Jpn. 71 (2002) p.1820.
[6] J.W.G Wildoer, L.C. Venema, A.G. Rinzler, R.E. Smalley and C. Dekker, Nature 391 (1998) p.59.
[7] T.W. Odom, J.L. Huang, P. Kim and C.M. Lieber, Nature 391 (1998) p.62.
[8] P. Kim, T.W. Odom, J.L. Huang and C.M. Lieber, Phys. Rev. Lett. 82 (1999) p.1225.
[9] M. Ouyang, J.L. Huang, C.L. Cheung and C.M. Lieber, Science 292 (2001) p.702.
[10] H. Kataura, Y. Kumazawa, Y. Maniwa, I. Umezu, S. Suzuki, Y. Ohtsuka and Y. Achiba, Synth. Met. 103 (1999) p.2555.
[11] O. Jost, A.A. Gorbunov and W. Pompe, Appl. Phys. Lett. 75 (1999) p.2217.
[12] Y. Zhang, Y.W. Tan, H.L. Stormer and P. Kim, Nature 438 (2005) p.201.
[13] C. Berger, Z.M. Song, T.B. Li, X.B. Li, A.Y. Ogbazghi, R. Feng, Z.T. Dai, A.N. Marchenkov, E.H. Conrad, P.N. First and W.A. de Heer, J. Phys. Chem. B 108 (2004) p.19912.
[14] C. Berger, Z. Song, X. Li, X. Wu, N. Brown, C. Naud, D. Mayou, T. Li, J. Hass, A.N. Marchenkov, E.H. Conrad, P.N. First and W.A. de Heer, Science 312 (2006) p.1191.
[15] K. Nakada, M. Fujita, G. Dresselhaus and M.S. Dresselhaus, Phys. Rev. B 54 (1996) p.17954.
[16] P.J.F Harris, *Carbon Nanotubes and Related Structures: New Materials for the 21St Century*, Cambridge University Press, Cambridge, 1999.
[17] R. Bacon, J. Appl. Phys. 31 (1960) p.283.
[18] H. Shioyama and T. Akita, Carbon 41 (2003) p.179.
[19] L.M. Viculis, J.J. Mack and R.B. Kaner, Science 299 (2003) p.1361.
[20] J.G. Lavin, S. Subramoney, R.S. Ruoff, S. Berber and D. Tomanek, Carbon 40 (2002) p.1123.
[21] D. Tomanek, W. Zhong and E. Krastev, Phys. Rev. B 48 (1993) p.15461.
[22] D. Tomanek, Phys. B 323 (2002) p.86.
[23] S.F. Braga, V.R. Coluci, S.B. Legoas, R. Giro, D.S. Galvao and R.H. Baughman, Nano. Lett. 4 (2004) p.881.
[24] M. Fujita, K. Wakabayashi, K. Nakada and K. Kusakabe, J. Phys. Soc. Jpn. 65 (1996) p.1920.
[25] C.P. Chang, Y.C. Huang, C.L. Lu, J.H. Ho, T.S. Li and M.F. Lin, Carbon 44 (2006) p.508.
[26] K.H. Ahn, Y.H. Kim, J. Wiersig and K.J. Chang, Phys. Rev. Lett. 90 (2003) p.026601.
[27] T.S. Li, S.C. Chang, J.Y. Lien and M.F. Lin, Nanotechnology 19 (2008) p.105703.
[28] T.S. Li, M.F. Lin and S.C. Chang, J. Appl. Phys. 107 (2010) p.063714.
[29] Y.C. Huang, C.P. Chang and M.F. Lin, J. Appl. Phys. 103 (2008) p.073709.